RESEARCH PAPERS

Acta Cryst. (1994). D**50**, 793–807

Refined Crystal Structure of Liver Alcohol Dehydrogenase–NADH Complex at 1.8 Å Resolution

BY SALAM AL-KARADAGHI,* EILA S. CEDERGREN-ZEPPEZAUER† AND SVEN HÖVMOLLER

Department of Structural Chemistry, Arrhenius Laboratories for Natural Sciences, Stockholm University, S-106 91 Stockholm, Sweden

AND KYRIACOS PETRATOS,‡ HOWARD TERRY AND KEITH S. WILSON

European Molecular Biology Laboratory (EMBL), c/o DESY, Notkestrasse 85, D-22603 Hamburg, Germany

(*Received* 5 *August* 1993; *accepted* 16 *May* 1994)

Abstract

The crystal structure of the ternary complex of horse liver alcohol dehydrogenase (LADH) with the coenzyme NADH and inhibitor dimethyl sulfoxide (DMSO) has been refined by simulated annealing with molecular dynamics and restrained positional refinement using the program *X-PLOR*. The two subunits of the enzyme were refined independently. The space group was $P1$ with cell dimensions $a = 51.8$, $b = 44.5$, $c = 94.6$ Å, $\alpha = 104.8$, $\beta = 102.3$ and $\gamma = 70.6°$. The resulting crystallographic R factor is 17.3% for 62 440 unique reflections in the resolution range 10.0–1.8 Å. A total of 472 ordered solvent molecules were localized in the structure. An analysis of secondary-structure elements, solvent content and NADH binding is presented.

Introduction

Horse-liver alcohol dehydrogenase (LADH) (alcohol:NAD^+ oxidoreductase, E.C. 1.1.1.1) catalyzes the transfer of two electrons and one proton between primary or secondary alcohols and NAD^+. The enzyme is a dimer of two subunits each consisting of 374 amino acids (Jörnvall, 1970). Each subunit is divided into two domains – the catalytic domain with two Zn(II) ions and the coenzyme-binding domain which has a typical dinucleotide α/β fold (Brändén, Jörnvall, Eklund & Furugren, 1975; Rossman, Liljas, Brändén & Banaszak, 1975).

The physico-chemical properties of LADH have been extensively studied by biochemical and spectroscopic techniques. The three-dimensional structures of three conformational states of the protein have been studied by crystallographic methods (Zeppezauer, Söderberg, Brändén, Åkeson & Theorell, 1967; Eklund *et al.*, 1976; Eklund *et al.*, 1981; Cedergren-Zeppezauer, Andersson, Ottonello & Bignetti, 1985). These structures represent the apo-enzyme as well as complexes with NADH, coenzyme analogues, inhibitors or substrates (for reviews see Eklund & Brändén, 1983; Cedergren-Zeppezauer, 1986).

Depending on the crystallization conditions and on the presence of coenzyme, substrate or inhibitors, different crystal forms of LADH have been obtained. The apo-enzyme crystallizes in an orthorhombic space group ($C222_1$) with the two subunits of the dimer related by a crystallographic twofold axis. Ternary complexes with NADH and substrate or inhibitor bound to the active site of the enzyme form crystals in either space group $C222_1$, $P1$, $P2_1$ or $C2$ (Brändén, 1965; Zeppezauer, Söderberg, Brändén, Åkeson & Theorell, 1967; Eklund *et al.*, 1981). However, none of these structures were refined to high resolution. Thus, for the orthorhombic open-enzyme form data were collected to 2.4 Å resolution and refined to a crystallographic R factor of 19%, while the triclinic closed complex with NADH and the inhibitor dimethyl sulfoxide (DMSO) was only partially refined at 2.9 Å resolution.

The X-ray structures of the apo-enzyme and its complexes revealed two major conformational states. The open conformation of the apo-enzyme, characteristic of the orthorhombic crystals, and the closed consisting of the ternary complex with NADH and DMSO (space group $P1$). The two enzyme forms were found to be related to each other by a rigid-body rotation of the catalytic domains by about 10° with respect to the central core of the dimer and a

* Present address: Department of Molecular Biophysics, Lund University, Box 124, S-221 00 Lund, Sweden.

† Author for correspondence.

‡ Present address: Institute of Molecular Biology and Biotechnology, PO Box 1527, GR-71110 Heraklion, Greece.

ISSN 0907-4449

rotation of about 1° of the coenzyme-binding domains with respect to each other around an axis approximately perpendicular to the molecular twofold axis (Colonna-Cesari *et al.*, 1986).

The closed form of LADH has been observed only in monoclinic or triclinic crystal forms. The absence of a crystallographic twofold axis relating the subunits of the dimer in these space groups could be interpreted as an indication of coenzyme-induced asymmetry between the subunits (Brändén, Jörnvall, Eklund & Furugren, 1975). The structure of the ternary complex of LADH–NADH–DMSO clearly demonstrated the similarity of the overall fold of the two subunits after the conformational transition. However, the resolution of the X-ray model did not allow a detailed comparison of the two subunits to be performed. Recent developments in X-ray detection techniques combined with the high intensity of synchrotron radiation sources opened up possibilities for high-resolution good quality data from crystals of large protein complexes to be collected in a reasonable time. We present here the refined structure of the ternary complex of LADH with NADH and DMSO at 1.8 Å resolution. The refinement at this resolution permitted, for the first time, an accurate description of the parameters of secondary-structure elements, metal-coordination geometry, atomic displacement parameters and the solvent structure of the enzyme. The data are also used to solve the controversial question concerning subunit dissimilarities. The coordinates and structure factors have been deposited with the Protein Data Bank (Bernstein *et al.*, 1977).*

Crystallization, data collection and processing

The enzyme, horse-liver alcohol dehydrogenase, was purchased from Boeringer. Crystals of the complex of LADH with NADH and DMSO were prepared from 2-methyl 2,4-pentandiol (MPD) in 0.05 *M* Tris–HCl, pH 8.4 as described earlier (Eklund *et al.*, 1981). The space group is *P*1 and cell dimensions are $a = 51.8$, $b = 44.5$, $c = 94.6$ Å, $\alpha = 104.8$, $\beta = 102.3$ and $\gamma = 70.6°$.

Three-dimensional data were collected from three crystals at the EMBL beamline X31 at the DORIS storage ring, DESY, Hamburg. The ring was operating at 3.7 GeV and 40–90 mA with approximately 3 h between injections. The monochromator, a single crystal of Si channel-cut along the (111) face, provided monochromatic X-rays. The crystals were mounted on a φ-rotation axis of an Enraf–Nonius camera. Data collection proceeded at 277 K.

Table 1. *Summary of data collection*

Detector	Imaging plate of EMBL, Hamburg
X-ray source	Beamline X31
Wavelength of X-rays (Å)	$\lambda = 1.009$
Crystal size (mm)	
Crystal 1	2 × 0.9 × 0.7
Crystals 2 and 3	1 × 0.7 × 0.5
Collimator apertures (mm)	
Crystal 1	0.4 × 0.4
Crystals 2 and 3	0.3 × 0.3
No. of images	198
Oscillation range (°)	1 for crystal 1 3 for crystals 2 and 3
Total No. of measured reflections	194817
No. of unique reflections	62440
Resolution range (Å)	10–1.8
Completeness (%)	88.5
R_{merge}*	0.08
For the entire data set	
55369 reflections had $I > \sigma$ (88.7%)	
51105 reflections had $I > 2\sigma$ (81.8%)	
47426 reflections had $I > 3\sigma$ (76.0%)	

* The merging R factor is defined as $\sum|I_i - \langle I\rangle|/\sum I$, where I_i is an individual intensity measurement and $\langle I\rangle$ is the average intensity for this reflection.

Data were recorded using an imaging-plate scanner designed and built at the EMBL Hamburg outstation by J. Hendrix and colleagues. The scanner was controlled by a MicroVAX computer. Two-dimensional images were transferred directly to a computer disk for subsequent analysis and integration of the diffraction pattern. During the collection of high-resolution data many of the strong low-resolution reflections were saturated. Because of limitation by the dynamic range of the scanner, collection of more than one data set, each with a different exposure time, was necessary.

The images were evaluated with a modified version of the *MOSFLM* film-processing package (Leslie, Brick & Wonacott, 1986). Unless otherwise stated subsequent calculations were performed using the *CCP*4 program suite supplied by the SERC Daresbury Laboratory (1979). The *ROTAVATA/AGROVATA* programs were used to merge the data and to extract the unique set of reflections. The program *TRUNCATE* (French & Wilson, 1978) was used to convert the intensities to structure-factor amplitudes. Details of the data collection are presented in Table 1.

Restrained refinement

Initial model

The starting model for the refinement was the coordinate set of the triclinic ternary complex refined

* Atomic coordinates and structure factors have been deposited with the Protein Data Bank, Brookhaven National Laboratory (Reference: 2OHX, R2OHXSF). Free copies may be obtained through The Managing Editor, International Union of Crystallography, 5 Abbey Square, Chester CH1 2HU, England. (Reference: GR0277).

Table 2. *Course of the refinement of* Zn–*LADH*

Step	1	2*a*	2*b*	3	4	5	6	7
Resolution								
Lower limit (Å)	8.0	8.0	8.0	8.0	8.0	8.0	10.0	10.0
Higher limit (Å)	2.0	2.0	1.8	1.8	1.8	1.8	1.8	1.8
No. of reflections	45666	45666	62260	62260	62260	62260	62440	62440
Type†	*P*	SA + *P*	SA + *P*	SA + *P*	*P*	B_{anis}	*P*	*P*
SA temperature (K)		3000	3000	2000				
No. of cycles	60*	40	40	40	120	—	120	80
No. of waters	0	0	0	296	280	280	391	472
R value (%)	31.8	27.1	27.3	23.1	22.2	18.5	17.8	17.2

* The resolution was gradually increased in 0.2 Å steps from 3.0 to 2.0 Å with 60 cycles of refinement at each step.
† *P*, positional refinement; SA, simulated-annealing refinement. B_{anis}, overall anisotropic temperature-factor refinement.

by H. Eklund at 2.9 Å resolution (unpublished results). 13 solvent molecules were present in this model. The starting *R* factor calculated with the present data was 31.7% at 3.0 Å resolution. In order to investigate the possible differences between the two subunits of the enzyme, refinement was carried out treating the whole dimer independently without imposing any symmetry restraints on the subunits.

The structure was refined in several steps by a combination of positional refinement and simulated annealing with the program *X-PLOR* (Brünger, Karplus & Petsko, 1989) implemented on a Convex C201 computer. Standard *X-PLOR* topology and parameter files were employed in the refinement of the protein and the coenzyme NADH. Table 2 summarizes the course of the refinement.

Step 1. The initial structure was subjected to 60 cycles of positional refinement, which reduced the crystallographic *R* factor from 31.7 to 22.1% in the resolution range 8.0–3.0 Å. Successive extension of the refinement to 2.0 Å resolution in 0.2 Å steps with 60 cycles of positional refinement at each resolution interval was followed by 20 cycles of restrained *B*-factor refinement. The resulting crystallographic *R* factor was 31.8% in the resolution range 8.0–2.0 Å. Several test runs were performed to find the optimal number of cycles for the positional and *B*-factor refinements. We found the general procedure described by Brünger (1988) satisfactory with slight modification of the cycle numbers depending on the amount of the preceding model building and the resolution range.

Step 2. The refinement was continued with a simulated-annealing cycle run at 3000 K with the slow-cooling protocol (Brünger, Krukowski & Erickson, 1990) including structure-factor amplitudes in the resolution range 8.0–2.0 Å (Table 3). The positions of the Zn(II) ions in the model were fixed during this step and the following cycles of positional refinement with a harmonics potential constant of 418.4 kJ mol^{-1} $Å^{-2}$ (100 kcal mol^{-1} $Å^{-2}$). The van der Waals radii for the Zn(II) ions were kept artificially low (0.55 Å) to minimize contacts with the liganding cysteine S atoms, histidine N atom and DMSO O atom. This allowed the refinement to be carried out without application of restraints to the distances between the metal and its ligands. The crystallographic *R* factor was 30.2% after simulated annealing and 40 cycles of positional refinement. Another 20 cycles of restrained *B*-factor refinement brought the *R* factor to 27.1%. The following simulated-annealing cycle was run with a similar protocol, but with data in the extended resolution range 8.0–1.8 Å. The crystallographic *R* factor dropped from 30.4 to 29.1% after simulated-annealing and positional refinement and to 27.3% after restrained *B*-factor refinement.

Table 3. *Simulated-annealing refinement protocol for LADH*

Stage	Description
1	Determination of weight W_A
2	Positional refinement. $\Delta_F = 0.0$
3	Molecular dynamics, 1.5 ps, $T = 3000$ K (or 2000 K, see Table 2), time step = 1 fs, velocity scaling every 25 fs, $\Delta_F = 0.2$
4	Positional refinement, 40 cycles
5	Restrained *B*-factor refinement, 15 cycles

Notes: The total potential energy of the system in *X-PLOR* is given by $E_{tot} = E_i + E_x$, where the empirical energy term E_i is a function of all atomic positions of the system describing internal stereochemical interactions and E_x is an effective potential energy consisting of weighted differences between observed ($|F_o|$) and calculated ($|F_c|$) structure-factor amplitudes. $E_x = W_A/N_A \Sigma W_n \; [|F_o(\mathbf{h})| - k|F_c(\mathbf{h})|]^2$, where N_A is a normalization factor and W_A is an additional weight, which relates E_x to the empirical potential energy E_i. Δ_F indicates how far any atom can move before an update of the first derivatives of E_x is enforced (see Brünger *et al.*, 1989).

Step 3. $2F_o - F_c$ and $F_o - F_c$ maps were calculated and the model was rebuilt using *FRODO* (Jones, 1978) implemented on an Evans & Sutherland PS330 graphics station. The program *PEAKMAX* was used to locate potential solvent sites above the 3σ level of the $F_o - F_c$ map. The predicted sites were examined on the graphics screen and about 300 out of 500 located by the program were inserted into the model. The selection was based on several criteria – distance from the protein chain, distance from other solvent

molecules and hydrogen-bonding possibilities. A large number of positive peaks appeared in the $F_o - F_c$ density due to errors in protein-atom positions. All side-chain and main-chain atoms with poor or no density at the 1.5σ level of the $2F_o - F_c$ density map were assigned zero occupancy.

The model was subjected to a new cycle of simulated-annealing refinement at 2000 K with a slow-cooling protocol similar to the previous one. The positions of the water molecules were fixed by a harmonics potential constant 125.5 kJ mol^{-1} $Å^{-2}$ (30 kcal mol^{-1} $Å^{-2}$) and the harmonics energy term was switched on during all the following stages. The R factor after cooling, positional refinement and restrained B-factor refinement was 23.1%.

Step 4. Once again the model was inspected. About 100 water molecules were deleted from the structure as having high B values (> 80 $Å^2$). Residues 2–6 of the N-terminus of both subunits were extensively rebuilt using an omit $F_o - F_c$ density map. Other residues with poor density were also checked with a series of omit maps and rebuilt whenever the positions of the side chains were visible in the map. 84 new water molecules were included manually during the graphics sessions by inspection of the $F_o - F_c$ density map at the 3σ level. The model was refined with 120 cycles of positional refinement followed by 20 cycles of restrained B-factor refinement. The R factor dropped to 22.2%.

Step 5. After a few more sessions of rebuilding and refinement we were surprised to find that the R factor did not improve further and in some cases it even became higher. It seemed that the stucture was stuck in an incorrect local minimum. Several simulated-annealing cycles with different cooling protocols were run with data in different resolution shells, with and without water molecules, but all these efforts did not lead to any improvement in the R factor. As a result we had to doubt the correctness of the positive peaks in the $F_o - F_c$ density map, which were taken as guidelines during model-rebuilding sessions. It was noticed that some peaks appeared close to the heavier atoms of the structure [main-chain O atoms, cysteine and methionine S atoms, Zn(II) ions] and could not be removed by model rebuilding and refinement. The only explanation for this could be an inherent anisotropy of the experimental data (Sheriff & Hendrickson, 1987). A tendency of LADH diffraction data to possess anisotropy was observed earlier (Eklund *et al.*, 1981). When this was realized, 15 cycles of overall anisotropic B-factor refinement were carried out with *X-PLOR* and the calculated components of the overall anisotropic B factor were applied to the observed structure-factor amplitudes. The values of the anisotropic B-factor components (expressed in U_{ij}, where $B_{ij} = 8\pi U_{ij}$) were as follows: $U_{11} = -0.012$, $U_{22} = 0.04$, $U_{33} = 0.12$, $U_{12} = -0.01$, $U_{13} = -0.01$ and $U_{23} = 0.02$ $Å^2$. The subsequent restrained individual isotropic B-factor refinement with the corrected data set resulted in a significant decrease of the R value from 22.2 to 18.5%.

Step 6. The model was again inspected. Many of the spurious $F_o - F_c$ density peaks had now disappeared and this facilitated rebuilding of the structure. The main-chain atoms were generally in correct positions and did not need manual rebuilding except residues 1–3 at the N terminus of both subunits as well as residues 133–135 in the B subunit. These residues consitute a loop localized on the surface of the protein. However, the same loop was well resolved in the A subunit.

Some of the methionine residues were incorrectly built in earlier steps due to spurious positive densities around the S atoms in the map. Those were corrected. The number of water molecules was increased to about 400.

The model was subjected to 120 cycles of positional refinement and 20 cycles of individual isotropic B-factor refinement. The weighting factor W_A, which gives a relative weighting of the X-ray term with respect to stereochemical terms in *X-PLOR* was kept during the positional refinement at about twice the value calculated by the program. We felt that this gave a better convergence of the refinement, without leading to serious deterioration in model geometry (r.m.s. deviation of bond length from ideality increased from 0.019 to 0.023). The R factor after this stage was 17.8%.

Step 7. New density maps were calculated. Only those residues which were affected by the last rebuilding and those in which some of the atoms were assigned zero occupancy were inspected. About 50 new water sites were located. Some additional peaks were found close to CB atoms of residues Cys281 and Cys282 in both subunits. These peaks were not caused by errors in the model and were considered to be due to discretely disordered side chains. The positions of the alternative side-chain conformations were built into the model.

As mentioned earlier the two subunits of the LADH dimer were refined independently. Continuous checks during the course of the refinement showed that the conformations of the main- and side-chain groups in the subunits were approaching each other. During the final refinement step the r.m.s. differences between the side chains of the subunits were calculated and residues showing r.m.s. values higher than 0.5 Å were checked. Those which needed some correction in either of the subunits were rebuilt. Most of these residues were located on the surface of the protein. Residues with no density (occupancy = 0) were left in their positions and no attempts were made to bring them into similar con-

formations in the two subunits (see a later section for a comparison of both subunits).

The model was subjected to 80 cycles of positional refinement with the weighting factor W_A reset to the value calculated by *X-PLOR*. This was followed by 15 cycles of *B*-factor refinement. The final *R* value was 17.3% with all the measured data in the resolution range 10.0–1.8 Å included and with a total of 472 ordered solvent molecules in both subunits of the dimer. The occupancies of residues Cys281 and Cys282 in the *A* subunit and Cys281 in the *B* subunit were refined and gave approximate values of 0.2 and 0.8 for the two conformations.

The geometry of the final model was of good quality with r.m.s. deviations from ideality of 0.014 Å for bond lengths and 2.91 and 25.95° for bond angles and torsion angles, respectively.

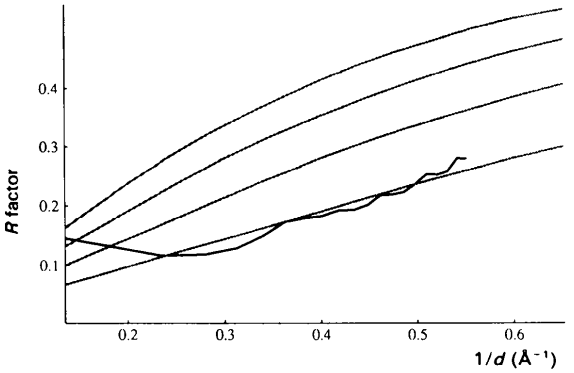

Fig. 1. The Luzzati plot of final *R* factor against resolution. The lines estimated for a series of average coordinate errors (0.2 to 0.5 Å) are also shown. The interception of the axes is at $1/d = 0.15$ Å^{-1}.

Quality of the model

Fig. 1. shows the Luzzati plot (Luzzati, 1952) for the refined structure of LADH. The average coordinate error estimated from the plot is about 0.24. This value is in good agreement with those found earlier for protein structures of similar resolution (Hubbard & Blundell, 1987).

The distribution of main-chain torsion angles (φ,ψ) for the LADH dimer are shown on the Ramachandran plot (Ramachandran & Sasisekharan, 1968) in Fig. 2. A contour map showing the core (inner lines) and the allowed regions (outer lines) of (φ,ψ) values as defined by Morris,

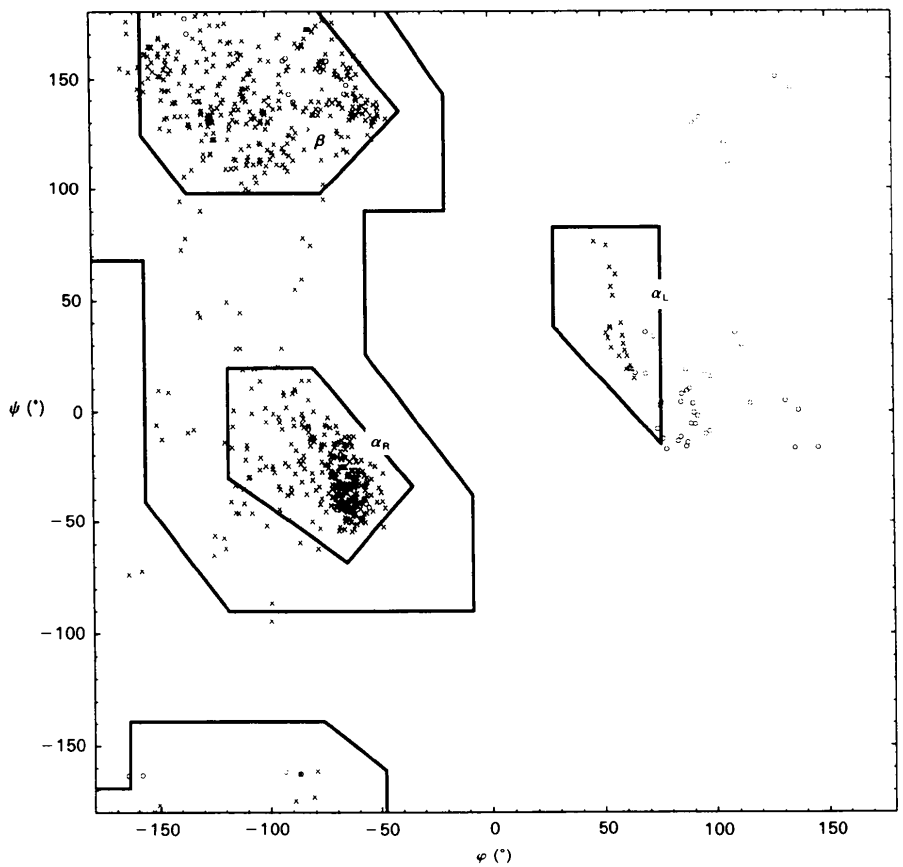

Fig. 2. The Ramachandran (φ, ψ) plot (Ramachandran & Sasisekharan, 1968) for the refined model of LADH–NADH–DMSO complex. Circles correspond to glycines, crosses to all other residues. The contour map corresponds to the core (inner lines) and allowed regions of (φ, ψ) values according to Morris, MacArthur, Hutchinson & Thornton (1992).

MacArthur, Hutchinson & Thornton (1992) is superimposed on the plot. The α/β nature of LADH is apparent from the two biggest clusters of points in the diagram.

Ten non-glycine residues from each subunit were found in the left-handed helical region of the Ramachandran plot: Lys18, His34, Arg133, Leu141, Ser144, Lys188, Asn259, Ser298, Phe319 and Lys338. All these residues are associated either with turns or positioned at the C-terminal ends of α-helices and will be discussed later. Isoleucine 368 with torsion angles of (-99, $-86°$) and (-99, $-95°$) in the *A* and *B* subunits, respectively, is in the high-energy region of the Ramachandran plot. It is positioned at a sharp corner where the protein backbone changes direction immediately before strand 3 (residues 369–374) of the sheet β-I. An extensive hydrogen-bonding network around Ile368 seems to contribute to the stabilization of this conformation. Thus, the main-chain NH groups of Ile368 and Arg369 make hydrogen bonds to OG1 of Thr347 and C=O of Leu345, while the C=O group of Arg369 forms a hydrogen bond to the main-chain NH of Thr347. Both C=O groups of Ile368 and Ser367 interact through solvent molecules with the coenzyme group O1PA. The conformation of the cysteine residues Cys174 in *A* (-158, $-72°$) and *B* subunits (-164, $-74°$) is essential for the coordination of the catalytic Zn(II).

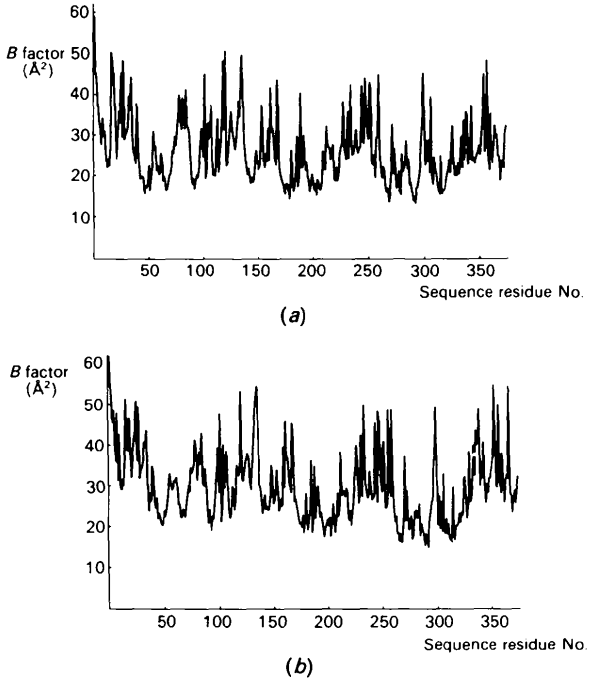

Fig. 3. The *B* factors (Å^2) averaged over side-chain atoms of the *A* (*a*) and *B* (*b*) subunits of LADH.

Table 4. *Side-chain atoms with undefined positions in the electron-density map after the refinement*

Subunit A					
Arg84	CD	NE	CZ	NH1	NH2
Lys5	CB	CG	CD	CE	NZ
Glu256,	CG	CD	OE1	OE2	
Lys135, 330	CG	CD	CE	NZ	
Lys10, 99, 104, 226	CD	CE	NZ		
Glu107, 366	CD	OE1	OE2		
Gln191	CD	OE1	NE2		
Met118	CG	SD	SE		
Ser1	CB	OG			
Lys8, 159, 185, 212, 248	CE	NZ			
Glu78	OE1	OE2			
Lys19, 159, 247, 339	NZ				
Subunit *B*					
Arg84	CD	NE	CZ	NH1	NH2
Lys5, 135	CG	CD	CE	NZ	
Glu17, 78, 107, 353	CG	CD	OE1	OE2	
Lys18, 99, 135, 226, 338	CD	CE	NZ		
Gln191	CD	OE1	NE2		
Met118	CG	SD	CE		
Ser1	CB	OG			
Lys113, 159, 248	CE	NZ			
Arg133	CZ	NH1			
Asn259	OD1	ND2			
Glu357	CG	CD			
Lys8, 39, 104, 330	NZ				

A plot of the temperature factors averaged over side-chain atoms *versus* residue number for the two subunits is presented in Figs. 3(*a*) and 3(*b*). The average *B*-factor value for all protein atoms is 27 Å^2 and with water molecules included is 29 Å^2. The average *B* values for the catalytic and coenzyme-binding domains were 24 and 27 Å^2 in the *A* subunit and 25 and 31 Å^2 in the *B* subunit, respectively. In comparison to other protein structures these values are rather high. A similar high average value of the *B* factors has been observed for the Cu(II)-substituted ternary complex of LADH (unpublished results). This probably depends on loose crystal packing in the lattice and on the anisotropy of the diffraction data (Kuriyan, Petsko, Levy & Karplus, 1986). The higher average *B* factor for the catalytic domain suggests significant interdomain fluctuations as was predicted earlier on the basis of conformation energy analysis (Colonna-Cesari *et al.*, 1986).

The values of the *B* factors correlate well with the location of the residues in the structure. Thus, the highest values are observed for surface loops and turns, while the lowest correspond to the active-site residues and parts of the nucleotide-binding region.

The electron-density map of the final model was of good quality with well resolved positions of the majority of main- and side-chain atoms. Residues with atoms for which there was no significant density are listed in Table 4. In total there were 49 residues in both subunits with one or more of their atoms missing in the electron density (about 130 out of

5568 atoms in the structure). Ten of these residues belong to the coenzyme-binding domain and the rest to the catalytic domain. All of these are exposed to solvent and their side-chain conformations are not restricted by interactions with other parts of the protein.

One particularly poor region of the electron-density map was that of the solvent-exposed turn consisting of residues Cys132–Lys135 in the *B* subunit. Both the main- and side-chain atoms of this turn lacked clear density and their positions could not be defined unambiguously. However, the hydrogen-bonding pattern is characteristic for a type I′ β-turn with C=O of Cys 132 hydrogen bonded to NH of Lys135 (2.81 Å).

The effect of the refinement at high resolution can be demonstrated by a least-squares superposition of the initial and final models. The mean r.m.s. differences for backbone and side-chain atoms were 0.54 and 1.35 Å (1.1 Å for all atoms) after the superposition of the CA atoms.

Some examples of the effect of the refinement on the atomic model are presented in Figs. 4 and 5. The conformation of the side chain of Gln124 is shown in Fig. 4 before and after the refinement together with the corresponding final electron-density map. The initial position of the side chain had considerable error for this residue. Fig. 5 shows helix α1 (residues Cys46–Thr56), which is located in the region of the active site of the enzyme and participates in Zn(II) coordination (Cys46) and in coenzyme binding. The positions of the CA atoms in the initial model agree well with those of the refined model, but the positions of the carbonyl O atom and side-chain atoms along the helix have shifted. As an example, the distance between the catalytically important OG of Ser48 and NE2 of His51 changed from 3.87 Å in the initial model to 5.05 Å after refinement.

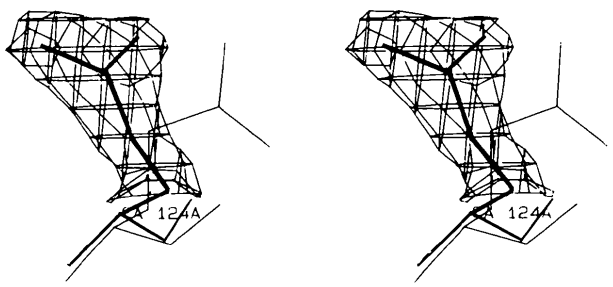

Fig. 4. A stereo plot showing the conformation of Gln124 before (thin lines) and after the refinement (thick lines) superimposed on $2F_o - F_c$ electron-density map at the 1.5σ level.

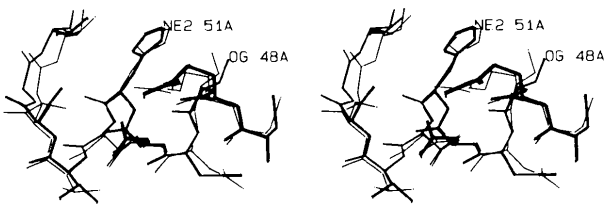

Fig. 5. A stereo plot of helix α1 (residues 46–56) is shown before (thin lines) and after the refinement (thick lines).

Description of the structure of LADH

The overall fold of the apo- and holo-forms of LADH and the interactions between the two subunits and between NADH and the protein have been presented earlier (Eklund *et al.*, 1976; Eklund *et al.*, 1981; Eklund, Samama & Jones, 1984). In this paper we focus on the analysis of the secondary-structure elements and the hydrogen-bonding pattern, metal-coordination geometry, solvent structure and on the comparison of the conformations of the two subunits in the enzyme. We also present an analysis of the interactions of the coenzyme with solvent molecules and protein groups.

Secondary-structure elements

The secondary-structure elements were defined using the program *DSSP* (Kabsch & Sander, 1983). The hydrogen-bonding pattern was checked with the program *HBOND* and additionally using *FRODO*. Main-chain hydrogen bonds were defined when C=O···N and O···H distances did not exceed 3.30 and 2.5 Å, respectively.

Distortions at the N- and C-termini of helices in protein structures are very common and need to be defined properly for correct secondary-structure assignments (Richardson & Richardson, 1989). Baker & Hubbard (1984) introduced a classification of α-helix terminal distortions based on the hydrogen-bonding pattern. We follow their classification. Residues forming 3_{10}- and π-type bonds at N- or C-terminal ends of helices were included in the definition of helices but not used in the calculation of the mean (φ,ψ) hydrogen-bond parameters.

The β-sheets were defined by the parallel or anti-parallel hydrogen-bonding pattern of neighbouring residues to another section of the polypeptide chain and by the respective torsional angles. We follow the notation used by Eklund *et al.* (1976) for helices and β-sheets except for the sheet forming the nucleotide-binding fold, which we refer to as β-NAD in the text. Unless stated otherwise, the individual (φ,ψ)

Table 5. *Summary of dihedral angles in helices and sheets in LADH with standard deviations for the respective parameters in parentheses*

	Residues	Mean φ (°)	Mean ψ (°)	Residues excluded from mean φ, ψ calculations
Helices				
$\alpha 1A$	46–56	−64 (4)	−34 (7)	Cys46 Gly55 Thr56
$\alpha 1B$		−64 (4)	−35 (6)	
$\alpha 2A$	165–176	−73 (3)	−24 (15)	Pro165 Cys174 Phe176
$\alpha 2B$		−73 (14)	−26 (19)	
αAA	177–189	−72 (15)	−43 (12)	Lys188 Val189
αAB		−73 (16)	−43 (12)	
αBA	201–216	−67 (7)	−38 (6)	Gly201 Ala214 Gly215
αBB		−65 (6)	−39 (6)	Ala216
αCA	225–237	−66 (6)	−38 (6)	Asn225 Lys226 Asp227
αCB		−65 (4)	−39 (9)	Val235 Gly236 Ala237
αDA	249–260	−64 (7)	−38 (10)	Pro249 Ser258 Asn259
αDB		−65 (5)	−37 (8)	Gly260
αEA	271–282	−64 (5)	−41 (8)	Arg 271 Cys281 Cys282
αEB		−67 (5)	−37 (8)	
$S3_{10}A$	304–311	−66 (16)	−33 (8)	Asn304 Gly311
$S3_{10}B$		−67 (15)	−31 (6)	
$\alpha 3A$	323–338	−65 (8)	−41 (5)	Lys323 Ala337 Lys338
$\alpha 3B$		−68 (9)	−39 (6)	
$\alpha 4A$	354–365	−63 (9)	−38 (11)	Lys354 Ser364 Gly365
$\alpha 4B$		−64 (8)	−38 (7)	
Overall mean		−65 (1)	−38 (3)	$\alpha 2$, αA and $S3_{10}$ excluded.
Sheets				
β-IA		−118 (26)	138 (21)	
β-IB		−122 (30)	138 (22)	
β-IIA		−112 (28)	138 (23)	
β-IIB		−110 (29)	143 (18)	
β-IIIA		−109 (27)	135 (25)	
β-IIIB		−107 (25)	134 (24)	
β-NADH (A)		−116 (28)	138 (17)	
β-NADH (B)		−115 (26)	138 (18)	
Overall mean		−114 (28)	138 (22)	

Table 6. *Summary of reverse-turn dihedral angles* (°)

	Residues	φ_2	ψ_2	φ_3	ψ_3	Type	Sequence in one-letter code
1A	Thr2···Lys5	−53	128	88	−17		
1B		−55	128	94	−5	II	TAGK
2A	Glu16···Lys19	−56	148	54	29		
2B		−60	141	65	15	II	EEKK
3A	Lys32···Glu35	−57	137	63	24		
3B		−56	136	63	21	II	KAHE
4A	Gly77···Val80	−59	144	86	−17		
4B		−58	135	87	2	II	GEGV
5A	Arg84···Asp87	−49	140	87	−16		
5B		−49	132	96	−10	II	RPGD
6A	Cys111···Asn114	−67	−11	−88	8		
6B		−64	−13	−91	8	I	CLKN
7A	Met123···Gly126	−62	−19	−94	11		
7B		−62	−28	−83	5	I	MQDG
8A	Cys132···Lys135	57	34	80	−21		
8B		53	39	74	−9	I′	CRGK
9A	Phe140···Thr143	54	34	68	17		
9B		49	35	62	20	I′	FLGT
10A	Asp153···Ser156	−56	−42	−61	−11		
10B		−61	−34	−70	−2	I	DEIS
11A	Asp161···Ser164	−68	−14	−95	10		
11B		−63	−28	−85	11	I	DAAS
12A	Thr190···Ser193	−61	131	92	0		
12B		−55	132	89	−5	II	TQGS
13A	Asn242···Asp245	−49	−27	−75	−11		
13B		−50	−35	−73	−8	I	NPQD
14A	Glu283···Tyr286	−71	−19	−100	−24		
14B		−70	−27	−91	−22	I	QEAY
15A	Pro296···Gln299	−48	133	58	21		
15B		−50	136	63	19	II	PDSQ
16A	Phe319···Phe322	59	23	77	0		
16B		65	18	77	3	I′	FGGF
17A	Leu342···Leu345	−52	−38	−54	−25		
17B		−54	−40	−52	−25	III	LDPL
18A	Asp343···Ile346	−54	−25	−83	−21		
18B		−52	−25	−87	−21	III	DPLI
19A	Pro351···Lys354	−49	−36	−67	−17		
19B		−53	−33	−62	−24	III	PFEK

values presented in the text refer to the A subunit of the enzyme. The respective values for the B subunit are usually very close to those of the A subunit.

Helices

Each LADH subunit contains nine helices, four of which are located in the catalytic domain and the remaining five contribute to the formation of the nucleotide-binding fold. Table 5 lists the mean (φ,ψ) values for the helices. The overall mean (φ,ψ) values calculated excluding helices $\alpha 2$, αA and S_{10} were $(-65, -38°)$. These agree well with the values $(-65, -39°)$ presented by Morris, MacArthur, Hutchinson & Thornton (1992) from the analysis of 119 well refined ($R \leq 20\%$) high-resolution (≤ 2.0 Å) structures. The mean hydrogen-bonding parameters for the LADH–NADH–DMSO complex, 3.02 and 2.09 Å for N···O and H···O distances and 155, 140° for N—H···O and H···O=C angles, respectively, agree well with the respective values presented by Baker & Hubbard (1984): 2.99, 2.06 Å and 155, 147°.

Helices $\alpha 1$, $\alpha 2$ and αD form α_N-type distortions with a 3_{10}-bond. Helices $\alpha 3$ and $\alpha 4$ immediately follow turns 16 and 19 (Table 6). Probably for this reason they do not need to form additional 3_{10}-bonds and, therefore, begin with a normal α-helical bond. Helices αB and αE also start with an i, $i+4$ bond type, while helix αC starts with two 3_{10}-type bonds followed by a normal α-helical bond. All the residues with C=O groups involved in the first 3_{10}-type bond are in the β-region of the Ramachandran plot.

Compared to the N-terminal ends of the helices there is less diversity in the type of distortions observed at the C-terminal ends. Thus, helices $\alpha 1$, $\alpha 3$ and $\alpha 4$ from the catalytic domain and helices αB, αC, αD from the coenzyme-binding domain all end with a 1–6 bond (π-type). This is followed by a 2–5 bond with residue 5 in helices $\alpha 1$, $\alpha 3$, $\alpha 4$, αB and αD (Gly55, Lys338, Gly365, Lys188, Gly215 and Asn259) being in the α_L conformation (α_{c2}-distortion). Helices αD and αE also have a final

hydrogen bond of 3_{10}-type, but the C=O groups of the preceding residues (Ala278 and Leu307) are hydrogen bonded to the side-chain groups Ser265 and Arg312.

Helices $\alpha 1$, $\alpha 2$ and αA are of special interest. Helix $\alpha 1$ (residues 46–56) is the first helix along the sequence and is located in the catalytic domain (Fig. 5). One face of the helix is exposed on the surface of the enzyme and the other side forms part of the active site and is also at the interface between the two domains of the subunit. A hydrogen bond at this interface has been formed as the result of overall conformational change upon NADH binding between main-chain C=O of Thr56 and NH of Asp297, a residue in the flexible loop 292–299. The S atom of Cys46 provides one of the ligands to the catalytic Zn(II) ion and several main-chain and side-chain groups form hydrogen bonds to NADH – main-chain NH, NH2 and NE of Arg47, OG of Ser48 and NE of His51. The side chain of Arg47 also participates in an intrahelical salt bridge with Asp50. Asp49, which is buried in the interior of the protein, makes a hydrogen bond to the active-site His67 and a deeply enclosed water molecule.

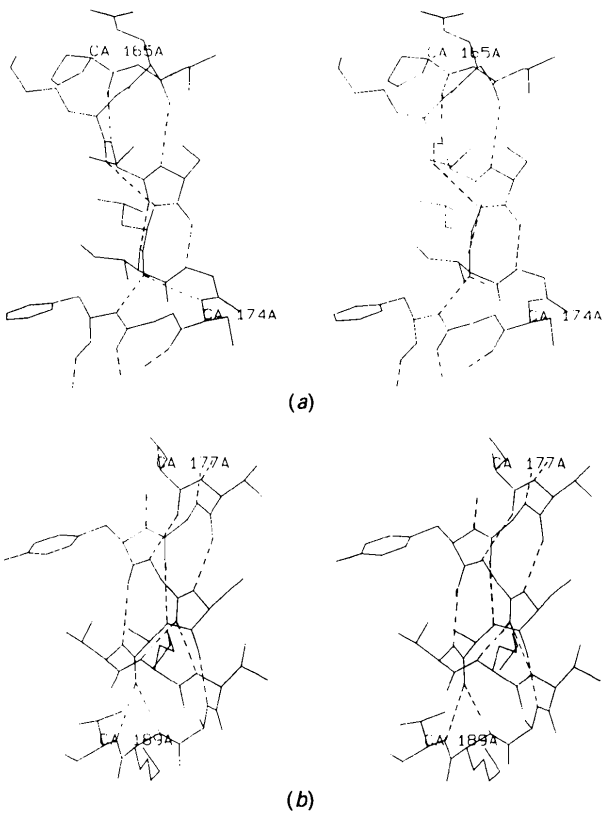

Fig. 6. A stereo plot of helices $\alpha 2$ (*a*) and αA (*b*) (residues 165–176 and 177–189). Residues 181–189 constitute a π-helix of about 1.5 turns. Dotted lines show the hydrogen bonds.

The hydrogen-bonding pattern of $\alpha 1$ is distorted at several locations. The C=O group of Cys46 forms a 3_{10}-type hydrogen bond with the NH group of Asp49 and the NH group of residue 48 is at a distance of 3.4 Å to SG46, possibly donating a proton to the S atom. The hydrogen bonds formed by the side-chain OG of Ser48, O2′N of NADH and the O atom of DMSO stabilize the conformation of Ser48. The distortions of the main-chain hydrogen-bonding pattern observed in this helix might depend on the interactions with the coenzyme, the inhibitor and the zinc-metal centre, but for definite conclusions to be made a well refined high-resolution structure of the apo-form of LADH is required.

The second helix comprising residues 165–189 is divided into two halves – helix $\alpha 2$ (residues 165–176, Fig. 6*a*), which belongs to the catalytic domain and αA (residues 177–189, Fig. 6*b*) forming the link to the coenzyme-binding domain (Eklund *et al.*, 1976). Cys174 provides the second sulfur ligand to the active site Zn(II) ion and together with Gly173 and Gly175 forms a kink at the end of helix $\alpha 2$ (Fig. 6*a*). The (φ, ψ) angles in the *A* subunit for Gly173 and Gly175 are (-66, $-21°$) and (-58, $-49°$), respectively, and for Cys174 (-158, $-72°$). The hydrogen bond between the NH group of Gly175 and OE2 of Glu68 and the bifurcated bond between C=O from Cys174 to OG1 and NH of Thr178 seem to be of primary importance for stabilizing this conformation. It should be noted that Glu68, a second buried acidic residue around the zinc centre, is among the most conserved residues in a variety of alcohol dehydrogenases (Borrás, Persson & Jörnvall, 1989).

The mean (φ, ψ) values (Table 5) for helix $\alpha 2$ are in the 3_{10} region of the Ramachandran plot. Three main-chain groups make hydrogen bonds only to solvent molecules; C=O and NH from Glu167, and C=O of Gly173. There are also two intrahelical side-chain to main-chain hydrogen bonds: OG of Ser177 to C=O of Ile172 and SH of Cys170 to the backbone amide N atom of the same residue.

Helix αA contains a π-helix of approximately 1.5 turns comprising residues 181–189 (Fig. 6*b*). The C=O group of Gly181 makes a bifurcated hydrogen bond to NH of Lys185 and Val186. The two carbonyl O atoms of Ser182 and Ala183 interact with NH of Ala187, Lys188 and Val189 (the last being a 1–7 bond). The C=O groups of residues Ala184, Ala187, Lys188 and Val189 are solely hydrogen bonded to solvent molecules, whereas the C=O group of Lys185 is bonded to NZ of Lys188. The mean N···O and H···O bond distances for residues Gly181–Ala187 are 3.09 (0.13) and 2.21 (0.23) Å and the mean (φ, ψ) are [-78 (17), -41 (14)°]. These differ significantly from the values for an ideal π-helix (-57, $-70°$) calculated by Low & Grenville-Wells (1953).

Table 7. *Metal–ligand distances and angular parameters for the ternary complex of LADH*

Atoms	Angle (°) *A* subunit	Angle (°) *B* subunit		Distance (Å) *A* subunit	Distance (Å) *B* subunit
Catalytic Zn(II)$_c$ centre					
SG46···*M*···NE67	114	112	SG46···*M*	2.23	2.20
SG46···*M*···SG174	130	130	SG174···*M*	2.32	2.26
NE67···*M*···SG174	105	108	NE67···*M*	2.15	2.04
SG46···*M*···O(DMSO)	105	103	O(DMSO)···*M*	2.26	2.13
SG174···*M*···O	103	102			
NE67···*M*···O	93	94			
Non-catalytic Zn(II)$_n$ centre					
SG97···*M*···SG100	108	105	SG97···*M*	2.37	2.40
SG97···*M*···SG103	113	117	SG100···*M*	2.32	2.36
SG100···*M*···SG111	119	118	SG103···*M*	2.27	2.30
SG100···*M*···SG103	107	106	SG111···*M*	2.34	2.39
SG103···*M*···SG111	108	107			
SG111···*M*···SG97	101	104			

β-sheets

There are four β-sheets in each subunit of LADH. Three of them form the core of the catalytic domain (β-I, β-II and β-III, notation of Eklund *et al.*, 1976). The fourth is a six-stranded sheet of the coenzyme-binding domain (β-NAD). The mean dihedral angles for the sheets are listed in Table 5. The average hydrogen-bonding parameters were 2.95 and 2.00 Å for N···O and H···O distances, and 159 and 151 for N—H···O and H···O=C angles, respectively. These values are almost identical to those found by Baker & Hubbard (1984) for β-sheets (2.91 and 1.96 Å, 160 and 151°).

A comparison of the structures of the refined ternary complex with that of the apo-enzyme (Eklund *et al.*, 1976) revealed some differences in the hydrogen-bonding pattern between the strands constituting sheets β-I and β-II. For this reason we modified the definition of the sheets and follow the Protein Data Bank numbering of the strands. We included strands 68–70, 41–45, 369–374 and 345–352 (numbers 1, 2, 3 and 4, respectively) in sheet β-I and strands 148–152, 35–40, 71–77, 86–92 and 156–160 (numbers 1, 2, 3, 4 and 5, respectively) in sheet β-II. The two last strands belonged to sheet β-I in the apo-enzyme structure. It is unclear whether the new hydrogen-bonding pattern is a result of the transition from the open to the closed form of LADH or reflects a more accurate definition of secondary-structure elements at high resolution.

Sheet β-III, which is a six-stranded β-barrel, only needed some minor modification and consists of strands 7–13, 22–29, 129–132, 62–66, 135–138 and 145–146. Sheet β-NAD is built up of strands 238–241, 215–223, 192–199, 262–268, 287–293 and 313–317.

Strands 4 of β-I and 3 of β-II include a bulge at Thr347 and Glu74 with (φ, ψ) angles (−103, −21°) and (−91, −49°), respectively. Residue Thr347 is positioned at a sharp corner directly after turns 17 and 18 (Table 6) which includes Leu342–Ile346 and serves in altering the direction of the backbone of strand 4. Four of the residues in the strands of sheet β-NAD also have dihedral angles in the helical region – Ala217 (−84, −26°), Thr238 (−85, −32°), Asp263 (−76, −40°) and Val292 (−115, −34°). These residues (with the exception of Thr238) are at the second position either from the beginning or end of the respective strands.

Tight turns

19 turns characterized by an (i, $i+3$) hydrogen bond were found in the structure of LADH. These were classified according to Richardson (1981) and Wilmot & Thornton (1988). The values of the dihedral angles of the second and third residues, which make the basis for the classification, are listed in Table 6. With the exception of turns 1, 6 and 15, the remaining turns are associated with the β-sheet regions of the structure. Turn 1 is at the N-terminus and turn 6 is in the core of the second zinc-binding lobe. Turn 15 is located in the middle of a flexible loop 294–297, which is crucial for the conformational transition of the protein (Cedergren-Zeppezauer, Andersson, Ottonello, Bignetti, 1985).

The type I′ turns all have Gly in the $i+2$ position. Type II turns have Gly in this position in three cases, one His (turn 3) and one Ser (turn 15). Main-chain and side-chain groups in all the turns make between two and four additional hydrogen bonds to main-chain or side-chain atoms from other parts of the structure or to solvent molecules. Turns 9 and 16 are internal; turn 16 participates in NADH binding and makes a hydrogen bond to a buried solvent molecule.

Table 8. *Classification of the ordered water molecules in the ternary complex of LADH*

Type	*A* subunit No.	*A* subunit $\langle B \rangle$ (Å^2)	*B* subunit No.	*B* subunit $\langle B \rangle$ (Å^2)
(*a*) Total in both subunits	244		228	
(*b*) Making 4 hydrogen bonds	39	40	39	39
(*c*) Making 3 hydrogen bonds	60	41	46	42
(*d*) Making 2 hydrogen bonds	55	52	58	55
(*e*) Making 1 hydrogen bond	57	60	55	62

Table 9. *Protein–water interactions in LADH crystals*

Protein atoms	No. of waters	Mean distance (Å)	$\langle B \rangle$ (Å^2)
Peptide CO			
A subunit	142	2.94 (0.26)	42
B subunit	125	2.97 (0.26)	43
Peptide NH			
A subunit	59	3.03 (0.15)	36
B subunit	53	3.03 (0.15)	37
Side-chain O			
A subunit	79	2.95 (0.26)	47
B subunit	70	3.00 (0.31)	47
Side-chain N			
A subunit	31	3.02 (0.22)	48
B subunit	35	3.05 (0.25)	47

Zn-*binding centres*

Table 7 lists the refined parameters of the metal-binding sites for the catalytic $Zn(II)_c$ and non-catalytic $Zn(II)_n$. The error in $M\cdots L$ (metal–ligand) bond length estimated from the $Zn(II)_n\cdots S$ distances in three LADH structures refined at high resolution independently and with similar refinement protocols [Cu(II)-substituted LADH–NADH–DMSO complex and apo-LADH, unpublished results] is 0.03 Å. This value is higher than the respective values for the restrained protein bond lengths (0.014). The $M\cdots L$ distances for SG46, NE67 and O(DMSO) are very close to each other and shorter than the $Zn(II)_c\cdots$SG174 distance. The same longer bond distance was observed for SG174 in the open form of LADH (Eklund *et al.*, 1976). The $M\cdots L$ distances for the non-catalytic $Zn(II)_n$ ion are typical for $Zn(II)\cdots S$ complexes with tetrahedral coordination (2.252–2.496 Å) in small-molecule crystal structure (Vedani & Huhta, 1990). A comparison of the $L\cdots M\cdots L$ angles between the catalytic and non-catalytic metals shows that the geometry of the non-catalytic $Zn(II)_n$ centre is much closer to a tetrahedral geometry than that of the catalytic $Zn(II)_c$ site. One reason for that could be the homogeneous ligand sphere of the non-catalytic $Zn(II)_n$ ion.

The hydrogen-bonding pattern around the active-site $Zn(II)_c$ has been described earlier (Eklund, Jones & Schneider, 1986). However, there are some differences in the present refined model. The O atom of the inhibitor DMSO is within hydrogen-bonding distance of NE2 of His67 (3.11 Å) and OG of Ser48 (2.64 Å). This implies that both Ser48 and His67 might participate in orienting the substrate when it is bound to the metal. The hydrogen bond from the substrate through Ser48 to OQ2 of NADH is thought to be part of a proton-relay system of LADH.

Solvent structure

A total of 244 and 228 ordered solvent molecules could be detected in the *A* and *B* subunits, respectively. The assignment to each subunit was made on the basis of the nearest protein group to which the respective water molecule made contact. Water sites with *B* factors up to 75 Å^2 were included in the refinement and subsequent analysis. At the end of the refinement an $F_o - F_c$ map was calculated with those water molecules having $B > 75$ Å^2 omitted. All of these sites were located at the surface of the protein. The water molecules were deleted from the structure if no $F_o - F_c$ density could be observed at the 3σ level.

Table 8 presents the classification of the water sites and Table 9 describes the interactions between the protein and water for those water molecules that are directly hydrogen bonded to the protein. It can be seen from Table 9 that the majority of the water molecules are bound to O atoms in the protein, while about 25% are bound to N atoms. The mean distances of water molecules to protein groups are within the limits observed for hydrogen-bonding contacts.

Coenzyme binding

The nicotinamide moiety binds in the interior of the protein about 15 Å from the surrounding solvent, while the ADP–ribose-binding site is close to the surface of the enzyme. This difference is reflected in the average temperature factors of the two parts, 15 and 22 Å^2, respectively. From the values of the torsion angles of the coenzyme bound to the two subunits (Table 10, for definitions see Reddy, Saenger, Mühlegger & Weimann, 1981) it is seen clearly that the conformations of the two NADH molecules are identical. The puckering of the ribose sugar rings is C2′-*endo*. This was clearly seen in the electron-density map.

A schematic drawing showing hydrogen-bonding interactions between NADH, the enzyme and solvent

Table 10. *Torsion angles (°) of NADH bound to subunits A and B of LADH*

Torsion angle	Adenosine *A*	Adenosine *B*	NMN–ribose* *A*	NMN–ribose* *B*
O4′—C1′—N9—C8	78	78		
O4′—C1′—N1—C6			76	74
O4′—C1′—N9—C4	−103	−103		
O4′—C1′—N1—C2			−97	−102
C4′—O4′—C1′—C2′	−37	−37	−27	−32
O4′—C1′—C2′—C3′	41	42	41	44
C1′—C2′—C3′—C4′	−31	−31	−39	−40
C2′—C3′—C4′—O4′	10	10	25	22
C3′—C4′—O4′—C1′	17	16	1	6
C3′—C4′—C5′—O5′	−68	−76	49	52
O4′—C4′—C5′—O5′	176	169	−69	−64
O2′—C2′—C3′—O3′	−28	−27	−37	−42

Pyrophosphate chain	*A*	*B*
C4′A—C5′A—O5′A—PA	156	155
C5′A—O5′A—PA—OP3	76	86
PN—OP3—PA—O5′A	95	89
PA—OP3—PN—O5′N	−167	−160
OP3—PN—O5′N—C5′N	61	59
PN—O5′N—C5′N—C4′N	−169	−166

* NMN–ribose = nicotinamide ribose.

is presented in Fig. 7. Protein–coenzyme interactions in the two subunits were identical. About 16 water molecules are involved directly or indirectly (through other groups) in interactions with the coenzyme. The majority of these are located in the region around the pyrophosphate bridge. Several new features of the interactions of NADH with the protein were revealed by the refinement at high resolution. Among those in the adenine part of the coenzyme are the hydrogen bonds from N7A and the ribose O2′A through solvent molecules to NH1 of Arg271 and ND2 of Asn225, respectively (Fig. 7). In the nicotinamide moiety there is a bond between O3′N and the main-chain NH of Val294. This last interaction together with the bonds between main-chain C=O of Val292 and N7N of the carboxamide and NH of Asp297 with Thr56, respectively, should be crucial for stabilizing the conformation of the loop region 292–298. The movement of this loop is necessary for the rearrangement of the domains during the transition to the closed form of LADH.

Several new NADH contacts were observed between the catalytic domain and the pyrophosphate bridge. It is seen from Fig. 7 that the O atoms O1PA, O2PA, O1PN and O2PN are involved in an extensive hydrogen-bonding network, which includes several solvent molecules, main- and side-chain groups from the catalytic and coenzyme-binding domains. It seems that the pyrophosphate forms a bridge between the domains of the subunits and between the N- and C-terminal parts of the catalytic domain. Two major interaction areas between the coenzyme and the catalytic domain can be discerned from the present model. One is made up of the residues from helix α1 (Arg47, Ser48 and His51) and the other from Leu362 (helix α4) and residues Ser367, Ile368 and Arg369 belonging to a loop preceding the N-terminal strand 369–374 of sheet β-I. Apparently these interactions are important for the conformational transition to the closed form of LADH.

Comparison of the two subunits

The data presented above for secondary-structure elements, hydrogen-bonding pattern, solvent structure and metal-coordination geometry show clearly the close similarity of the conformations of the two subunits of LADH at the level of secondary-structure and hydrogen-bonding parameters. A residue-by-residue comparison was carried out by calculating the r.m.s. differences for main- and side-chain atoms after a least-squares superposition of the subunits using the CA atoms of the polypeptide backbone (program *X-PLOR*). The mean r.m.s. difference for the final model was 0.22 Å for backbone atoms and 0.34 Å for side chains. Atoms with undefined positions listed in Table 4 were excluded from the comparison. The r.m.s. values obtained from the comparison between the subunits can be used as an independent estimate of coordinate errors and is comparable with the error predicted from the Luzzati plot, which was about 0.24 Å. The corresponding r.m.s. differences for the starting model were 0.65 and 1.48 Å for main-chain and side-chain atoms, respectively. From these results it can be concluded that within the experimental error the two subunits are identical.

Concluding remarks

The present structure of the ternary complex of LADH is the first to be refined at high resolution. Many main-chain and side-chain atom positions were defined with much higher accuracy, allowing for substantial improvements to be made to the model. The new model permitted a more precise description of the secondary-structure elements, of the internal parameters of the structure and solvent interactions with the protein and with the coenzyme.

The two subunits of the enzyme could be compared with higher accuracy.

The new features observed for the interactions of NADH with the protein provide some clues regarding the coenzyme role in the conformational transition of LADH. It was noted that Ile368 in the present structure had main-chain torsion angles in the high-energy region of the Ramachandran plot (-99, $-86°$). However, the refinement of apo-LADH at high resolution (unpublished results) showed that the same angles were well inside the allowed region of the plot (-77, $-48°$). In the ternary complex of LADH with NADH and imidazole the enzyme remains in its open conformation (Cedergren-Zeppezauer, 1983). The newly performed refinement of this complex showed that (φ, ψ) angles of Ile368 in this case are (-71, $-70°$). Thus, not only NADH binding, but also the transition to the closed state is needed for the creation of a steric strain in this region of the polypeptide chain. In their analysis of steric strain in the polypeptide backbone of protein molecules, Herzberg & Moult (1991) showed that the relatively few sterically strained conformations almost always have some functional significance. However, additional studies will be needed to understand the mechanism behind the creation and release of such a strain.

An interesting question, which could be resolved after the refinement of the present model, concerned the possibility of the presence of solvent molecules in the substrate channel of LADH. It was established that the oxidation of the alcohol group of the sub-

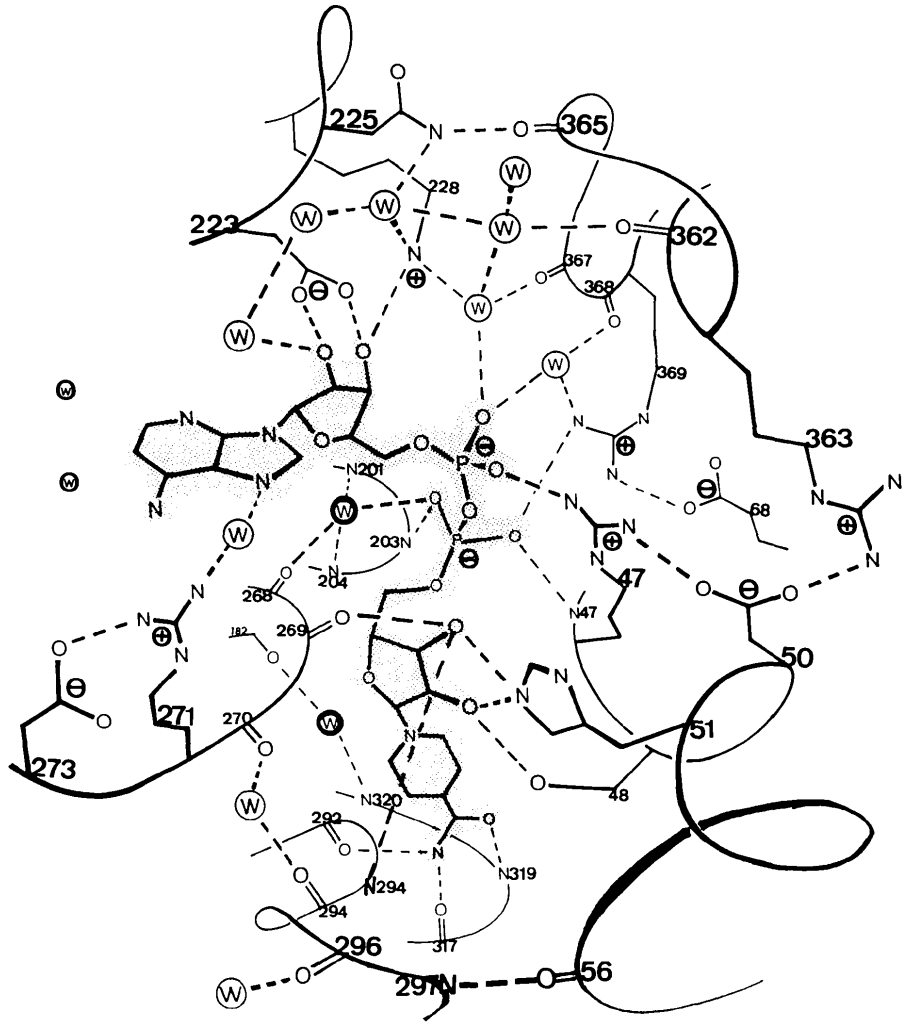

Fig. 7. A schematic drawing showing the NADH molecule (shaded) and its interactions with solvent and protein main-chain and side-chain groups. Dotted lines are hydrogen bonds. The drawing was designed by Bo Furugren.

strate occurs by a transfer of a hydride ion from the C1 atom that binds the hydroxyl group to the C4 atom of the oxidized form of the coenzyme. One of the requirements for the hydride transfer to occur is a hydrophobic environment in the neighbourhood of the metal ion and in the substrate channel that connects the active site with the surface of the molecule (Eklund & Brändén, 1983). The channel is approximately cylindrical, about 7 Å in diameter and 20 Å deep. It includes the so-called 'bottle-neck' region lined by hydrophobic side chains of residues Leu116, Leu141, Val294 and Ile318, approximately 8–10 Å away from the active-site zinc ion. Molecular dynamics simulations (Tapia, Eklund & Brändén, 1986) demonstrated that the 'bottle-neck' region serves as an effective barrier preventing the penetration of solvent molecules into the substrate channel. The present refined structure of the ternary complex of LADH confirmed these results. The volume of the substrate channel from the metal ion to the 'bottle-neck' region was found to be solvent free. The water molecule predicted by Tapia, Eklund & Brändén, (1986) to exist just outside the 'bottle neck' was found in the structure. It is positioned about 12 Å from the metal ion and does not make any hydrogen bonds. Its temperature factor is rather high (59 $Å^2$), which probably reflects a low occupancy. Three other water molecules were found close to the surface of the molecule [13 to 15 Å from the Zn(II) ion]. One of them is hydrogen bonded to the carbonyl O atom of Pro295 and to the second water molecule which in turn makes a bond to a third one.

The comparison of the refined high-resolution structures of the holo- and apo-forms of LADH will provide more detailed information regarding the conformational transition from the open to the closed states of the enzyme and the possible effects associated with crystal packing in different crystal forms. This work is in progress.

We are grateful to Professor H. Eklund for providing the coordinates of the ternary complex of LADH, which were used as a starting model in the refinement and to Dr Z. Dauter for assistance in data processing. This research was supported by the Swedish Science Research Council and Sven och Ebba-Christina Hagbergs Stiftelse.

References

BAKER, E. N. & HUBBARD, R. E. (1984). *Prog. Biophys. Mol. Biol.* **44**, 97–179.

BERNSTEIN, F., KOETZLE, T., WILLIAMS, G., MEYER, E., BRICE, M., RODGERS, J., KENNARD, O., SHIMANOUCHI, T. & TASUMI, M. (1977). *J. Mol. Biol.* **112**, 535–542.

BORRÁS, E., PERSSON, B. & JÖRNVALL, H. (1989). *Biochemistry*, **28**, 6133–6139.

BRÄNDÉN, C.-I. (1965). *Arch. Biochem. Biophys.* **122**, 215–217.

BRÄNDÉN, C.-I., JÖRNVALL, H., EKLUND, H. & FURUGREN, B. (1975). *The Enzymes*, Vol. 11, edited by P. D. BOYER, pp. 103–190, New York: Academic Press.

BRÜNGER, A. T. (1988). *J. Mol. Biol.* **203**, 803–816.

BRÜNGER. A. T., KARPLUS, M. & PETSKO, G. A. (1989). *Acta Cryst.* A**45**, 50–61.

BRÜNGER, A. T., KRUKOWSKI, A. & ERICKSON, J. W. (1990). *Acta Cryst.* A**46**, 585–593.

CEDERGREN-ZEPPESAUER, E. (1983). *Biochemistry*, **22**, 5761–5722.

CEDERGREN-ZEPPEZAUER, E. (1986). *Zinc Enzymes*, edited by I. BERTINI, C., LUCHINAT, W. MARET & M. ZEPPEZAUER, pp. 393–415. Boston: Birkhäuser.

CEDERGREN-ZEPPEZAUER, E., ANDERSSON, I., OTTONELLO, S. & BIGNETTI, E. (1985). *Biochemistry*, **23**, 4000–4010.

COLONNA-CESARI, F., PERAHIA, D., KARPLUS, M., EKLUND, H., BRÄNDÉN, C.-I. & TAPIA, O. (1986). *J. Biol. Chem.* **261**, 15273–15280.

EKLUND, H. & BRÄNDÉN, C.-I. (1983) *Zinc Enzymes*, edited by T. G. SPIRO, pp. 125–152. New York: John Wiley.

EKLUND, H., JONES, T. A. & SCHNEIDER, G. (1986). In *Zinc Enzymes*, edited by I. BERTINI, C. LUCHINAT, W. MARET & M. ZEPPEZAUER, pp. 393–415, Boston: Birkhäuser.

EKLUND, H., NORDSTRÖM, B., ZEPPEZAUER, E., SÖDERLUND, G., OHLSSON, I., BOIWE, T., SÖDERBERG, B.-O., TAPIA, O., BRÄNDÉN, C.-I. & ÅKESON, Å. (1976). *J. Mol. Biol.* **102**, 27–59.

EKLUND, H., SAMAMA, J.-P. & JONES, T. A. (1984). *Biochemistry*, **23**, 5982–5996.

EKLUND, H., SAMAMA, J.-P., WALLEN, L., BRÄNDÉN, C.-I., Åkeson, Å & Jones, T. A. (1981). *J. Mol. HBiol.* **146**, 561–587.

French, S. & Wilson, K. S. (1978). *Acta Cryst.* A**34**, 517–525.

JONES, T. A. (1978). *J. Appl. Cryst.* **11**, 614–617.

JÖRNVALL, H. (1970). *Eur. J. Biochem.* **16**, 25–40.

HERZBERG, O. & MOULT, J. (1991). *Proteins Struct. Funct. Genet.* **11**, 223–229.

HUBBARD, T. J. P. & BLUNDELL, T. L. (1987). *Protein Eng.* **1**, 159–171.

Kabsch, W. & Sander, C. (1983). *Biopolymers*, **22**, 2577–2637.

KURIYAN, J., PETSKO, G. A., LEVY, R. M. & KARPLUS, M. (1986). *J. Mol. Biol.* **190**, 227–254.

LESLIE, A. G., BRICK, P. & WONACOTT, A. J. (1986). *CCP4. News*, **18**, 33–39.

LOW, B. W. & GRENVILLE-WELLS, H. J. (1953). *Proc. Natl Acad. Sci. USA*, **39**, 785–801.

LUZZATI, V. (1952). *Acta Cryst.* **5**, 802–810.

MORRIS, A. L., MACARTHUR, M., HUTCHINSON, G. E. & THORNTON, J. M. (1992). *Proteins Struct. Funct. Genet.* **12**, 345–364.

RAMACHANDRAN, G. N. & SASISEKHAREN, V. (1968). *Adv. Prot. Chem.* **23**, 283–437.

REDDY, B. S., SAENGER, W., MÜHLEGGER, K. & WEIMANN, G. (1981). *J. Am. Chem. Soc.* **103**, 907–914.

RICHARDSON, J. S. (1981). *Adv. Prot. Chem.* **34**, 167–339.

RICHARDSON, J. S. & RICHARDSON, D. C. (1989). *Prediction of Protein Structure and the Principles of Protein Conformation*, edited by G. D. FASMAN, pp. 1–98. New York: Plenum Press.

ROSSMANN, M. G., LILJAS, A., BRÄNDÉN, C.-I. & BANASZAK, L. J. (1975). *The Enzymes*, Vol. 11, edited by P. D. BOYER, pp. 61–102, New York: Academic Press.

SERC Daresbury Laboratory (1979). *CCP4. A Suite of Programs for Protein Crystallography*, SERC Daresbury Laboratory, Warrington WA4 4AD, England.

SHERIFF, S. & HENDRICKSON, W. A. (1987). *Acta Cryst.* A**43**, 118–121.

TAPIA, O., EKLUND, H. & BRÄNDÉN, C.-I. (1986). In *Steric Aspects of Biomolecular Interactions*, edited by G. NÁRAY-SZABÓ & K. SIMIN. Florida: CRC Press.

VEDANI, A. & HUHTA, D. W. (1990). *J. Am. Chem. Soc.* **112**, 4759–4767.

WILMOT, C. M. & THORNTON, J. M. (1988). *J. Mol. Biol.* **203**, 221–232.

ZEPPEZAUER, E., SÖDERBERG, B.-O., BRÄNDÉN, C.-I., ÅKESON, Å. & THEORELL, H. (1967). *Acta Chem. Scand.* **2**, 1099–1101.